Influence of Skew and Cross-Coupling on Flux-Weakening Performance of Permanent-Magnet Brushless AC Machines

G. Qi[1,2], J. T. Chen[1], Z. Q. Zhu[1], *Fellow, IEEE*, D. Howe[1], L. B. Zhou[2], and C. L. Gu[2]

[1]Department of Electronic and Electrical Engineering, University of Sheffield, Sheffield S1 3JD, U.K.
[2]Department of Electrical Machines and Drives, Huazhong University of Science and Technology, Wuhan, Hubei 430074, China

A method is proposed for predicting the flux-weakening performance of permanent-magnet (PM) brushless ac machines accounting for skew and d-q axis cross-coupling. The method is based on a d-q-axis flux-linkage model, a hybrid 2-D finite-element (FE)–analytical method being used to predict the d- and q-axis inductances. However, it only requires 2-D FE analysis of the magnetic field distribution over a cross section of the machine. The developed method is used to predict the torque-speed characteristic of an interior PM brushless ac machine with one stator slot-pitch skew. This is compared with predictions from a direct FE analysis of the machine and validated by measurements.

Index Terms—**Cross-coupling, flux-weakening, inductances, magnetic saturation, optimal control, permanent-magnet machine, skew.**

I. Introduction

PERMANENT-MAGNET (PM) brushless ac (BLAC) machines exhibit a high torque density and are being employed for many applications, including aerospace and automotive, for which a high electric loading, together with forced liquid-cooling, may be desirable. Hence, the armature reaction can be significant and may affect the electromagnetic performance, in terms of the d- and q-axis inductances and the torque, due to magnetic saturation and the influence of d-q axis cross-coupling. The electromagnetic performance is also influenced by skew, which is often employed to achieve a sinusoidal back-emf waveform and to reduce the cogging torque and torque ripple.

The influence of cross-coupling magnetic saturation in electrical machines was analyzed in [1]–[3], and an equivalent circuit which accounted for saturation was presented in [4]–[6]. Since the influence of cross-coupling in synchronous reluctance machines is particularly significant, their d- and q-axis inductances and torque, accounting for saturation, have been investigated [7]–[10]. However, in PM BLAC machines, the stator flux-linkage is due to two sources, viz. the permanent magnets and the armature reaction. In order to determine the influence of cross-coupling on the performance, the nonlinear permeability distribution was determined under a specified load condition, and to enable the d- and q-axis inductances to be subsequently obtained from a linear calculation [11], [12]. However, this approach is not particularly convenient, and indeed is not possible with some commercial finite element (FE) packages, although some of them can do this, such as Jmag and Ansys FE packages. Therefore, in this paper a simpler method for predicting the d- and q-axis flux-linkages, the electromagnetic torque and the terminal voltage is proposed. Hence, it can be readily employed to determine the flux-weakening performance with due account for the influence of cross-coupling magnetic saturation, which is often neglected [13], [14].

As regards skew, numerous papers have accounted for its influence on the air-gap flux density distribution, the back-emf waveform, the cogging torque, torque ripple, and the average torque [15]–[18]. An analytical skew factor was employed in the air gap flux density for machines with skew [19]. In addition, a hybrid 2-D FE—analytical method was proposed to predict the d- and q-axis inductances of PM BLAC machines with skew [20], albeit neglecting the influence of cross-coupling. In this paper, an improved analytical method is developed to account for cross-coupling and skew. It is employed to predict the d- and q-axis inductances and torque-speed characteristic of a skewed interior PM (IPM) BLAC machine in the flux-weakening mode of operation, and validated by measurements.

II. Torque Calculation Accounting for Cross-Coupling Magnetic Saturation

The electromagnetic torque of a PM BLAC machine can be calculated from [21]

$$T = \frac{3}{2}p[\psi_d I_q - \psi_q I_d] \tag{1}$$

or

$$T = \frac{3}{2}p\left[\psi_{PM} I_q + (L_d - L_q) I_d I_q\right] \tag{2}$$

where p is the number of pole-pairs, Ψ_d and Ψ_q are the d- and q-axis flux-linkages, Ψ_{PM} is the PM flux-linkage, I_d and I_q are the d- and q-axis currents, and L_d and L_q are the d- and q-axis inductances.

Under flux-weakening control, the maximum output torque capability is determined by the phase voltage and current limits, viz.

$$U_a = \sqrt{U_d^2 + U_q^2} \le U_{\max} \tag{3}$$

$$I_a = \sqrt{I_d^2 + I_q^2} \le I_{\max} \tag{4}$$

$$U_d = -\omega L_q I_q + R I_d \text{ or } U_d = -\omega\psi_q + R I_d \tag{5}$$

$$U_q = \omega(\psi_{PM} + L_d I_d) + R I_q \text{ or } U_q = \omega\psi_d + R I_q \tag{6}$$

Manuscript received June 04, 2008; revised January 10, 2009. Current version published April 17, 2009. Corresponding author: Z. Q. Zhu (e-mail: Z.Q. Zhu@sheffield.ac.uk).

Color versions of one or more of the figures in this paper are available online at http://ieeexplore.ieee.org.

Digital Object Identifier 10.1109/TMAG.2009.2013244

where U_a and I_a are the phase terminal voltage and current, respectively, U_d and U_q are the d- and q-axis voltages, respectively, ω is the electrical angular velocity, and R is the phase resistance.

The maximum phase current is limited by the rated supply current, whilst the maximum phase voltage can be estimated from the dc link voltage when a hysteresis pulse-width modulated controller is employed [22]

$$U_{\max} = \frac{2}{\pi} U_{dc}. \tag{7}$$

In order to simplify the control strategy, the phase resistance can be neglected in (5) and (6), but the associated voltage drop can subsequently be compensated for in the voltage limit. The voltage limit, can, thus, be expressed by [23]

$$U'_a = \sqrt{U'^2_d + U'^2_q} \le U'_{\max} = U_{\max} - RI_a \tag{8}$$

where

$$U'_d = -\omega L_q I_q \text{ or } U'_d = -\omega \psi_q \tag{9}$$

$$U'_q = \omega(\psi_{PM} + L_d I_d) \text{ or } U'_q = \omega \psi_d. \tag{10}$$

Various methods for predicting the torque-speed characteristic, corresponding to alternative definitions of the flux-linkages and inductances, are available, as follows.

A. Constant Parameter Method

The PM flux-linkage and the d- and q-axis inductances are simply assumed to be constant, and the influence of magnetic saturation is neglected, i.e.,

$$\psi_{PM}(0) = \psi_d(I_d = 0, I_q = 0) \tag{11}$$

$$L_d(0) = \frac{\psi_d(I_d = \Delta I_d, I_q = 0) - \psi_d(I_d = 0, I_q = 0)}{\Delta I_d} \tag{12}$$

$$L_q(0) = \frac{\psi_q(I_d = 0, I_q = \Delta I_q)}{\Delta I_q} \tag{13}$$

where ΔI_d and ΔI_q are incremental d- and q-axis currents, typically 5% of the rated current.

The torque and voltage are predicted from (2) and (8) for specified vales of the d- and q-axis current. For IPM BLAC machines, the relationship between the d- and q-axis currents for maximum torque can be derived from $\partial T / \partial I_d| = 0$ [24], as

$$I_d = \frac{\psi_{PM}(0)}{2\left(L_q(0) - L_d(0)\right)} - \sqrt{\frac{\psi^2_{PM}(0)}{4\left(L_q(0) - L_d(0)\right)^2} + I_q^2} \tag{14}$$

$$I_d^2 = I_{\max} - I_q^2. \tag{15}$$

In the flux-weakening operating region, the relationship for maximum power can be derived from $U_a = U'_{\max}$, viz.

$$I_d = -\frac{\psi_{PM}(0)}{L_d(0)} + \frac{1}{L_d(0)} \sqrt{\frac{U'^2_{\max}}{\omega^2} - \left(L_q(0) I_q\right)^2} \tag{16}$$

where $|I_q| \le U'_{\max}/(\omega L_q)$.

However, although being simple and easy to implement, since ψ_m, L_d, and L_q are constant, the error in the predicted performance may be significant, especially if a high electric loading is employed and magnetic saturation due to armature reaction is significant.

B. Partial-Coupling Method

In order to improve the accuracy of the performance prediction, the influence of the q-axis current on the PM flux-linkage is accounted for, as well as the influence of the d- and q-axis currents on the d- and q-axis inductances, respectively, i.e.,

$$\psi_{PM}(I_q) = \psi_d(I_d = 0, I_q) \tag{17}$$

$$L_d(I_d) = \frac{\psi_d(I_d) - \psi_{PM}(0)}{I_d} \tag{18}$$

$$L_q(I_q) = \frac{\psi_q(I_q)}{I_q}. \tag{19}$$

The variation of Ψ_d with I_q, due to magnetic saturation, can be obtained directly by FE analysis. However, the analytical determination of the optimized d- and q-axis currents cannot be obtained so easily. Hence, optimized values predicted from the constant parameter method are employed to obtain the torque-speed characteristic in [24]. However, a large error may still result. Therefore, a simple program may be used to predict the optimized d- and q-axis currents by scanning values of I_d and I_q within the current limit (4). The voltage which results with the identified optimal currents can be obtained according to (8), and must meet the voltage limit, the corresponding torque being predicted from (2).

Although the partial-coupling method accounts to some extent for the influence of magnetic saturation, the electromagnetic performance can be influenced significantly by d-q axis cross-coupling.

C. Flux-Linkage Method

Since the torque and voltage can be obtained from the d- and q-axis flux-linkages (1), (8)–(10), $\psi_d(I_d, I_q)$ and $\psi_q(I_d, I_q)$ can be determined directly by FE analysis and used to accurately predict the torque-speed characteristic accounting for d-q cross-coupling, the d- and q-axis currents again being scanned to optimize I_d and I_q from which to determine the torque-speed characteristic. However, it remains difficult to predict the d- and q-axis flux-linkages by the FE method for machines with skew. Hence, a simplified method based on the foregoing flux-linkage method is proposed which uses the PM flux-linkage and the d- and q-axis inductances and currents to describe the d- and q-axis flux-linkages.

D. Proposed Method

The electromagnetic torque accounting for the influence of cross-coupling is given by

$$\begin{aligned} T &= \frac{3}{2} p \left[\psi_d(I_d, I_q) I_q - \psi_q(I_d, I_q) I_d\right] \\ &= \frac{3}{2} p \left[\psi_d(I_d = 0, I_q) I_q + \frac{\psi_d(I_d, I_q) - \psi_d(I_d = 0, I_q)}{I_d} I_d I_q \right. \\ &\qquad \left. - \frac{\psi_q(I_d, I_q)}{I_q} I_d I_q \right] \\ &= \frac{3}{2} p \left[\psi_{PM}(I_q) I_q + \left(L_d(I_d, I_q) - L_q(I_d, I_q)\right) I_d I_q\right] \end{aligned} \tag{20}$$

TABLE I
COMPARISION OF TORQUE CALCULATION METHODS

		Partial-coupling method	Flux-linkage method	Proposed method	Direct FE method
Ψ_{PM}	Constant	$f(I_q)$	--	$f(I_q)$	--
L_d	Constant	$f(I_d)$	--	$f(I_d, I_q)$	--
L_q	Constant	$f(I_q)$	--	$f(I_d, I_q)$	--
Ψ_d	--	--	$f(I_d, I_q)$	--	--
Ψ_q	--	--	$F(I_d, I_q)$	--	--
Optimized I_d & I_q	Analytical	Scanning	Scanning	Scanning	Scanning
Cross-coupling	--	Partial	Accurately	Accurately	Accurately

where

$$\psi_{PM}(I_q) = \psi_d(I_d = 0, I_q) \tag{21}$$

$$L_d(I_d, I_q) = \frac{\psi_d(I_d, I_q) - \psi_{PM}(I_q)}{I_d} \tag{22}$$

$$L_q(I_d, I_q) = \frac{\psi_q(I_d, I_q)}{I_q}. \tag{23}$$

The voltage U_a can be calculated from

$$U_a = \sqrt{(\omega L_q(I_d, I_q) I_q - RI_d)^2 + (\omega\psi_{PM}(I_q) + \omega L_d(I_d, I_q) I_d + RI_q)^2} = \sqrt{(\omega\psi_q(I_d, I_q) - RI_d)^2 + (\omega\psi_d(I_d, I_q) + RI_q)^2} \tag{24}$$

Similar to the partial-coupling method, the PM flux-linkage $\psi_{PM}(I_q)$ is obtained directly by FE analysis, although it should be noted that, in practice, Ψ_{PM} is also affected by I_d. However, it remains relatively difficult to predict since both the magnets and the stator current produce fluxes on the d-axis, although it can be obtained by predetermining the permeability distribution, as outlined earlier.

By employing, (20)–(23), as an alternative to (1), the problem of separating Ψ_{PM}, Ψ_d and Ψ_q is avoided. Clearly, however, Ψ_{PM}, L_d and L_q defined by (21)–(23) are only approximate. However, the electromagnetic torque and voltage obtained from (20)–(24) are accurate and identical to those predicted by the flux-linkage method accounting for the effect of cross-coupling magnetic saturation, but the calculation is significantly simpler for machines with skew, as will be shown in Section IV. The optimal values of I_d and I_q for maximizing the torque-speed characteristic can again be obtained by scanning the d- and q-axis currents.

Table I summarizes the features of the foregoing four approaches for predicting the torque-speed characteristic.

E. Direct FE Method

A further approach is to determine the torque-speed characteristic directly by FE analysis, using the Maxwell stress integration or virtual work methods [25]. In order to obtain the optimal d- and q-axis currents at each rotational speed, the variation of the torque and the voltage with the phase and magnitude of the current needs to be predicted. Clearly, when the predicted voltage is lower than the voltage limit, the maximum torque capability is obtained by comparing calculated torques for different current phase angles and magnitudes, and identifying the optimized values. This process, for the IPM BLAC machine whose specification is given in the Appendix, is illustrated in Figs. 1 and 2, for a specified speed of 3000 rpm and a current of magnitude 6 A. The variation of the line voltage with the current phase angle is first calculated and compared with the voltage limit in Fig. 1. As will be seen when the current phase angle $\geq \theta_o$, the line voltage is within the voltage limit, and the maximum torque is achieved when the current phase angle $= \theta_o$, as illustrated in Fig. 2, which shows the torque-current phase angle characteristic. However, since the current phase angle needs to be optimized at different current magnitude over the entire speed range, in order to maximize the torque-speed characteristic, the direct FE method is very time-consuming.

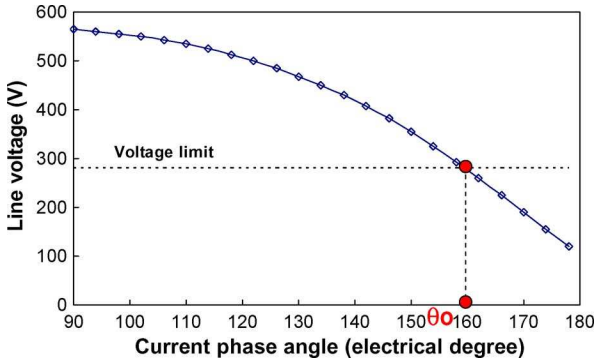

Fig. 1. Variation of FE predicted voltage with current phase angle, $I = 6$ A, 3000 rpm.

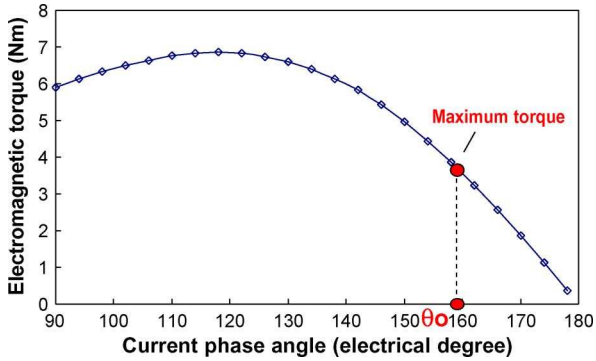

Fig. 2. Variation of torque with current phase angle, $I = 6$ A, 3000 rpm.

III. COMPARISON OF ELECTROMAGNETIC TORQUE PREDICTED BY ALTERNATIVE METHODS

Representative 2-D flux distributions for the IPM BLAC machine whose specification is given in the Appendix are shown in Fig. 3. Fig. 4 shows variations of the d- and q-axis flux-linkages with the d- and q-axis currents. The d-axis flux-linkage increases approximately linearly as I_d is reduced in magnitude, while the q-axis flux-linkage increases as I_q is increased, the rate of increase decreasing when $I_q > 4$ A due to the influence of saturation. The variation of Ψ_{PM} with I_q is shown in Fig. 5. As will be evident, Ψ_{PM} reduces as I_q is increased, again due to saturation.

Fig. 6 shows the variation of the d- and q-axis inductances, determined according to (21)–(23) and Figs. 4 and 5, accounting for cross-coupling. As will be seen, L_d increases slightly with an increase in the magnitude of I_d, and reduces significantly with

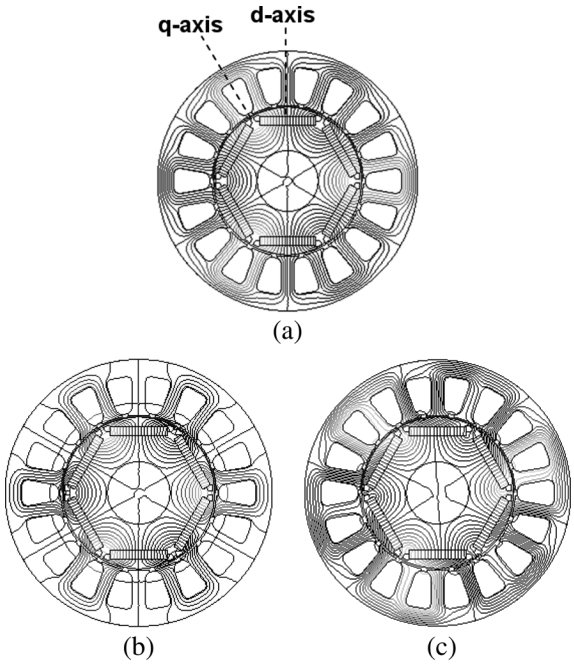

Fig. 3. Flux distributions. (a) Open-circuit; (b) $I_d = -6$ A, $I_q = 0$; and (c) $I_d = 0$, $I_q = 6$ A.

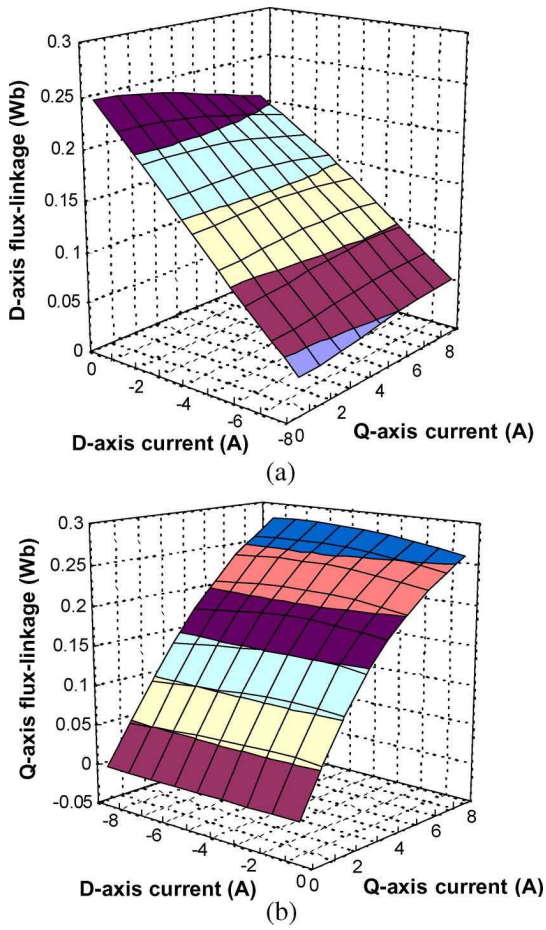

Fig. 4. D- and q-axis flux-linkages accounting for cross-coupling.

an increase of I_q. On the other hand, L_q reduces significantly with an increase of I_q and is less sensitive to I_d when I_q is large.

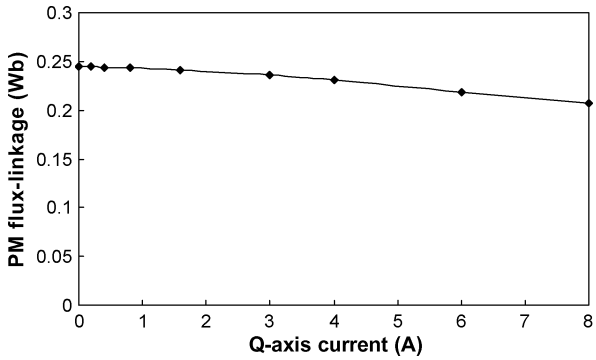

Fig. 5. Variation of PM flux-linkage with q-axis current.

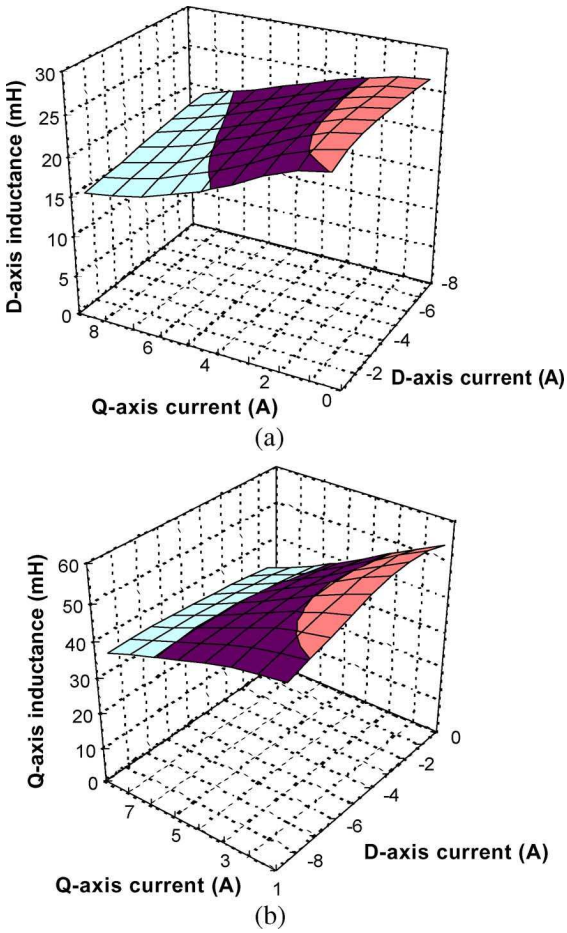

Fig. 6. D- and q-axis inductances accounting for cross-coupling.

The parameters for use in the foregoing five torque calculation methods are specified in Table II.

The optimized d- and q-axis currents of the IPM machine, as determined by the foregoing methods, are compared in Fig. 7 when $I_{max} = 6$ A, $U_{DC} = 279$ V, and $R = 8.5\ \Omega$ (100°C). As expected, the values predicted from the flux-linkage method and the proposed method are identical, and agree well with those obtained from the direct FE method over the entire operating speed range. However, they are significantly different from those predicted from the constant parameter and partial coupling methods. Moreover, the analytically optimized q-axis current is always lower than that obtained by scanning currents

TABLE II
PARAMETERS FOR TORQUE CALCULATION METHODS

	Constant parameter method	partial-coupling method	Flux-linkage method	Proposed method
Ψ_{PM}	Fig.5, I_q=0	Fig.5	--	Fig.5
L_d	Fig.6(a), I_d =I_q=0	Fig.6(a), I_q=0	--	Fig.6(a)
L_q	Fig.6(b), I_d =I_q=0	Fig.6(b), I_d =0	--	Fig.6(b)
Ψ_d	--	--	Fig.4(a)	--
Ψ_q	--	--	Fig.4(b)	--

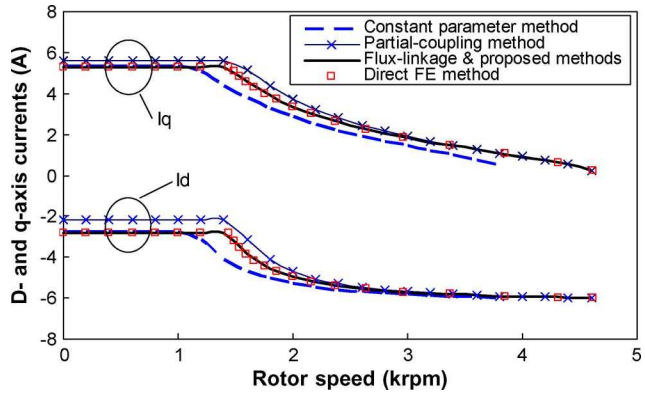

Fig. 7. Comparison of d- and q-axis currents, $I_{max} = 6$ A.

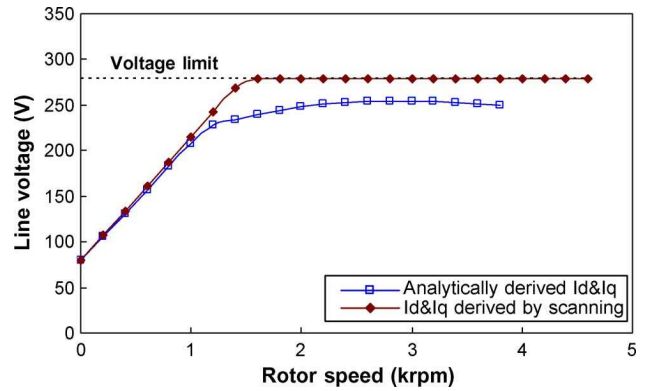

Fig. 8. Comparison of predicted line voltage by partial-coupling method, $I_{max} = 6$ A.

in the partial-coupling method. Fig. 8 compares the variation of the predicted line voltage by the partial-coupling method using the analytically optimized d- and q-axis currents and optimized values determined by scanning. As will be seen, at high speeds, i.e., in the flux-weakening region, when the analytically optimized currents are employed the line voltage is significantly lower than the voltage limit.

Predicted torque-speed characteristics are compared in Fig. 9. Again, good agreement is achieved between the torque predicted by the FE, flux-linkage and proposed methods. However, although the torque predicted in the flux-weakening region by the partial-coupling method employing d- and q-axis currents optimized by scanning is similar to that predicted by the FE flux-linkage and proposed methods, the value in the constant torque region is significantly lower. Further, when analytically

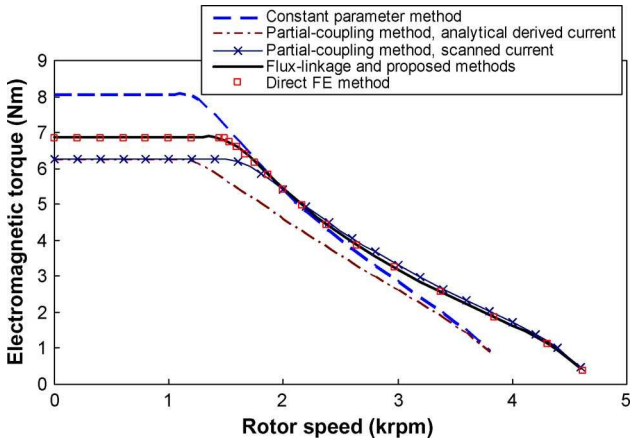

Fig. 9. Comparison of torque-speed characteristics, $I_{max} = 6$ A.

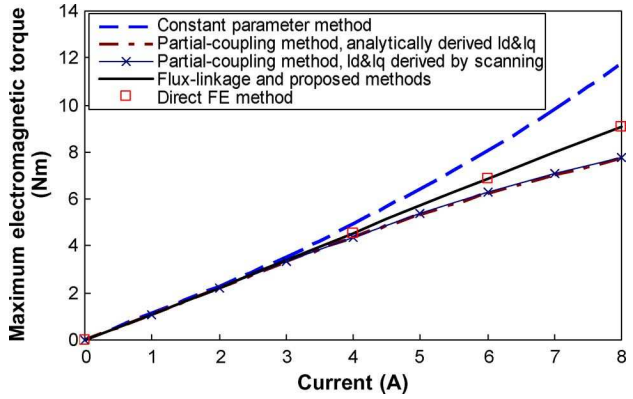

Fig. 10. Variation of maximum torque with current.

derived d- and q-axis currents are employed a large error in the predicted torque exists over the entire speed range. The predicted torque, and the d- and q-axis currents, are from the constant parameter method, quite different from those predicted from the direct FE method.

Fig. 10 compares the variation of the maximum torque with the current in the constant torque operating region as predicted by the different methods. As will be seen, whilst they are similar when the current is low, the difference increases as the current is increased and cross-coupling magnetic saturation becomes significant. The torque predicted by the constant parameter method is larger than that derived from the other methods due mainly to the neglect of the influence of I_q on Ψ_{PM}, whilst the lowest torque is predicted by the partial-coupling method.

IV. INFLUENCE OF SKEW

Skew is usually accounted for by sub-dividing the active length of the machine into several 2-D slices, analyzing each slice independently and then combining the predicted results [17]. Clearly, the positions of the d- and q-axes of each slice relative to the current will be different, as illustrated in Fig. 11. However, if the d- and q-axes of a skewed machine are assumed to be coincident with those of an unskewed machine at the center of the machine, the d- and q-axis flux-linkages produced

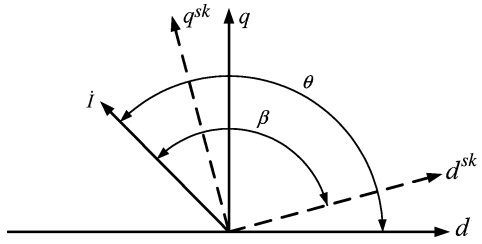

Fig. 11. Relative positions of d- and q-axes in unskewed and skewed machines.

by the armature reaction in the skewed machine, accounting for cross-coupling, can be obtained from

$$\psi_d^{sk} = \frac{1}{\alpha}\int_{\theta-\alpha/2}^{\theta+\alpha/2} \left[L_d^{2D}(I_d, I_q) I_d \cos(\theta-\beta) - L_q^{2D}(I_d, I_q) I_q \sin(\theta-\beta)\right] d\beta \quad (25)$$

$$\psi_q^{sk} = \frac{1}{\alpha}\int_{\theta-\alpha/2}^{\theta+\alpha/2} \left[L_d^{2D}(I_d, I_q) I_d \sin(\theta-\beta) + L_q^{2D}(I_d, I_q) I_q \cos(\theta-\beta)\right] d\beta \quad (26)$$

$$I_d = I_N \cos\beta \quad (27)$$

$$I_q = I_N \sin\beta \quad (28)$$

where sk signifies the machine with skew, 2-D signifies the machine without skew, α is the electrical skew angle, and θ and β are the current phase angles relative to the d-axes of the skewed and unskewed machines, respectively. I_N is the peak rated phase current, and $L_d^{2D}(I_d, I_q)$ and $L_q^{2D}(I_d, I_q)$ are the d- and q-axis inductances of the unskewed machine accounting for cross-coupling. It should be noted that L_d and L_q of the 2-D slices of the skewed machine vary with the axial position. However, if the skew angle is relatively small, this variation may be neglected. Thus,

$$L_d^{2D}(I_d, I_q) \approx L_d^{2D} = L_d^{2D}\left(I_N\cos(\theta), I_N\sin(\theta)\right) \quad (29)$$

$$L_q^{2D}(I_d, I_q) \approx L_q^{2D} = L_q^{2D}\left(I_N\cos(\theta), I_N\sin(\theta)\right). \quad (30)$$

Hence, the d- and q-axis flux-linkages and inductances can be derived from

$$\begin{aligned}\psi_d^{sk} &= \frac{1}{\alpha}\int_{\theta-\alpha/2}^{\theta+\alpha/2} \left[L_d^{2D} I_d \cos(\theta-\beta) - L_q^{2D} I_q \sin(\theta-\beta)\right] d\beta \\ &= \frac{L_d^{2D}}{2\alpha} I_N \cos\theta \cdot (\alpha + \sin\alpha) \\ &\quad + \frac{L_q^{2D}}{2\alpha} I_N \cos\theta \cdot (\alpha - \sin\alpha) \end{aligned} \quad (31)$$

$$\begin{aligned}\psi_q^{sk} &= \frac{1}{\alpha}\int_{\theta-\alpha/2}^{\theta+\alpha/2} \left[L_d^{2D} I_d \sin(\theta-\beta) + L_q^{2D} I_q \cos(\theta-\beta)\right] d\beta \\ &= \frac{L_d^{2D}}{2\alpha} I_N \sin\theta \cdot (\alpha - \sin\alpha) \\ &\quad + \frac{L_q^{2D}}{2\alpha} I_N \sin\theta \cdot (\alpha + \sin\alpha) \end{aligned} \quad (32)$$

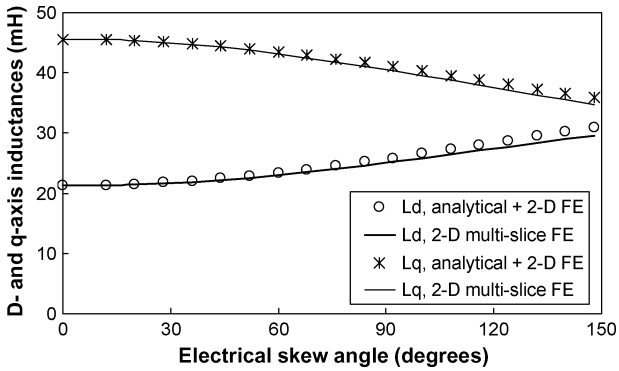

Fig. 12. Predicted d- and q-axis inductances with skew, $I_d = I_q = 4.25$ A.

$$L_d^{sk} = \frac{\psi_d^{sk}}{I_N\cos\theta} = L_d^{sk} + \frac{1-K_{sk}}{2}\left(L_q^{2D} - L_d^{2D}\right) \quad (33)$$

$$L_q^{sk} = \frac{\psi_q^{sk}}{I_N\sin\theta} = L_q^{sk} - \frac{1-K_{sk}}{2}\left(L_q^{2D} - L_d^{2D}\right) \quad (34)$$

$$K_{sk} = \frac{\sin\alpha}{\alpha} \quad (35)$$

where K_{sk} is the skew factor. It should also be noted that I_d and I_q are assumed to be constant in calculating the inductances L_d and L_q, (33) and (34). However, in the multi-slice machine model, I_d and I_q are different for each slice. Hence, the d- and q-axis inductances accounting for both skew and cross-coupling are obtained from the inductances determined without skew. However, they can also be predicted by FE analysis of the multiple 2-D slices according to (25) and (26). However, this is very time-consuming since I_d and I_q are different for each slice. Fig. 12 compares the d- and q-axis inductances predicted by (33) and (34) with those obtained by 2-D multislice FE analysis as the skew angle of the IPM machine is varied. As can be seen, values from the two methods are in good agreement, L_d increasing and L_q reducing as the skew angle is increased while the saliency ratio reduces.

The proposed analytical method for accounting for the influence of skew has also been employed to predict the d- and q-axis inductances of the IPM machine, whose parameters are given in the Appendix, with one stator slot-pitch skew, L_d and L_q being derived directly from Fig. 6 by using (33)–(35), whilst Ψ_{PM} is obtained from Fig. 5 by employing the skew factor (35). The optimal current-speed and torque-speed characteristics of the skewed machine accounting for cross-coupling can, thus, be obtained. By way of example, Figs. 13 and 14 compare the predicted characteristics with those of the unskewed machine. Again, the direct FE method has been employed to validate the predictions, the skewed machine being subdivided into 15 slices to predict its voltage and torque. As will be evident, the flux-weakening capability is improved as the L_d is increased due to skew, although the torque in the constant torque region is reduced since Ψ_{PM} and the saliency ratio are reduced.

V. Experimental Validation

The proposed methods for accounting for the influence of cross-coupling and skew have been validated by measuring the torque-speed characteristic of the IPM machine, whose end-winding inductance is 6.9 mH [20], and employing on-line optimal flux-weakening control [26].

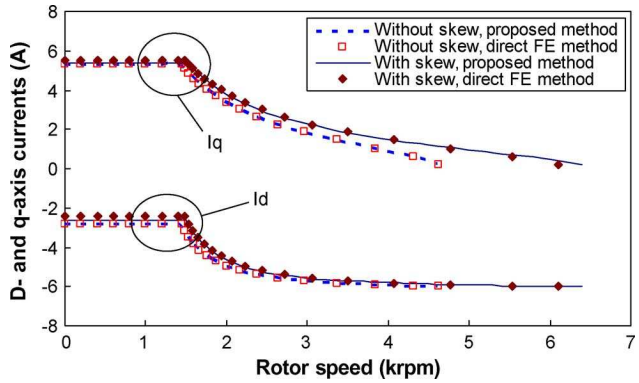

Fig. 13. Current-speed characteristics of IPM machine with and without skew, $I_{max} = 6$ A.

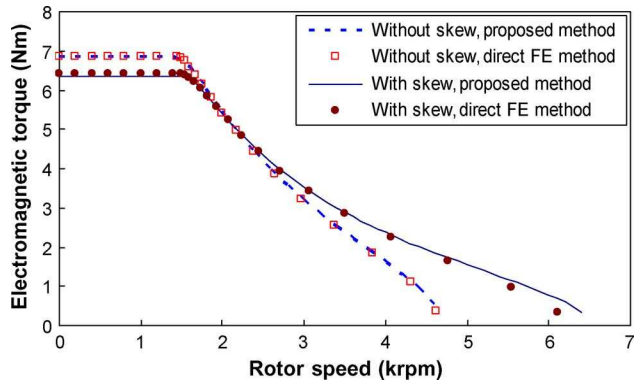

Fig. 14. Torque-speed characteristics of IPM machine with and without skew, $I_{max} = 6$ A.

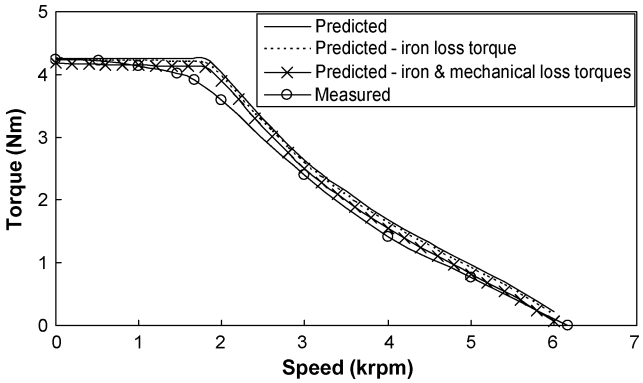

Fig. 15. Comparison of predicted and measured torque-speed characteristics of IPM machine with one slot pitch skew.

However, the actual shaft torque is less than the predicted electromagnetic torque due to the influence of iron loss and mechanical loss. Thus, in order to make a meaningful comparison of the predicted and measured results, the mechanical loss was measured by driving a dummy nonmagnetic rotor, whilst the iron loss was predicted by FE analysis [27], [28].

Fig. 15 compares measured and predicted torque-speed characteristics when the current limit is 4 A. As will be seen, good agreement is achieved when the iron and mechanical loss torques are subtracted from the predicted electromagnetic torque.

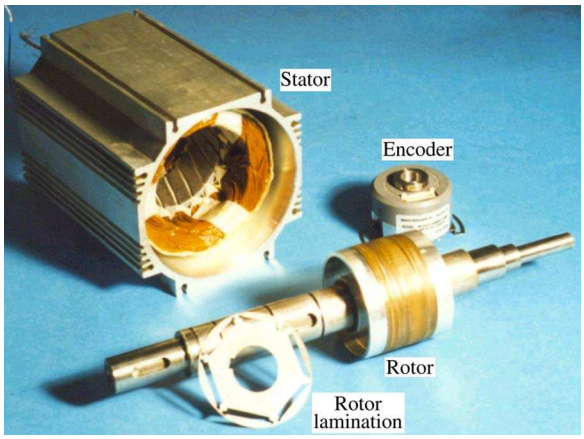

Fig. 16. The 6-pole, 18-slot IPM machine.

TABLE III
MAIN PARAMETERS OF IPM MACHINE

Number of phases	3
Number of poles	6
Number of slots	18
DC link voltage	570 V
Rated voltage (peak)	340 V
Rated current (peak)	4.0 A
Rated power	1.3 kW
Rated speed	3000 rpm
Rated torque	4.0 Nm
Outer diameter of stator	106.6mm
Inner diameter of stator	62.0mm
Airgap length	0.75mm
Active length	30.0mm
PM thickness	3.50mm
Magnet remanence	1.17 T
Relative permeability of magnets	1.07
Number of turns/phase	152
Phase resistance	6.0Ω (20℃), 8.5Ω (100°C)

VI. CONCLUSION

A simplified method for predicting the torque and voltage of PM brushless ac machines, accounting for cross-coupling, has been proposed. The determined electromagnetic performance agrees well with that predicted directly by FE analysis. In addition, a hybrid 2-D FE-analytical method, which requires only a single 2-D FE analysis has been developed to account for the influence of both skew and cross-coupling. It has been shown that when the skew angle is increased, L_d increases while L_q reduces. Thus, the flux-weakening capability of the machine is improved, while the maximum torque capability is reduced due to the reduction in Ψ_{PM} and the saliency ratio.

The proposed methods have been validated against the measured maximum torque-speed characteristic of an IPM BLAC machine with one slot pitch skew.

APPENDIX

Fig. 16 shows a prototype 6-pole, 18-slot IPM BLAC machine whose main parameters are given in Table III. The stator has a skew of 1 slot pitch. The line back-emf waveform was obtained by multi-slice FE analysis and is compared with the

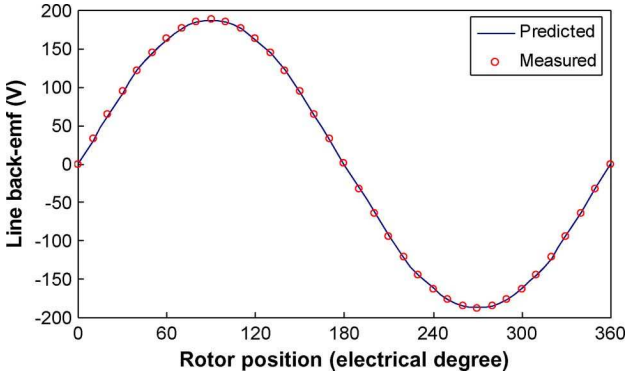

Fig. 17. Open-circuit line back-emf waveform, 1500 rpm.

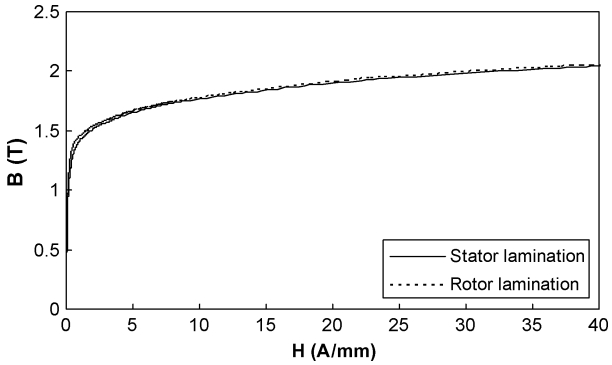

Fig. 18. B-H curves of stator and rotor lamination materials.

measured waveform in Fig. 17. The B-H curves of the stator and rotor lamination materials are shown in Fig. 18.

ACKNOWLEDGMENT

The first author gratefully acknowledges the China Scholarship Council for providing financial support for a one-year visiting Ph.D. studentship at The University of Sheffield.

REFERENCES

[1] A. M. El-Serafi and J. Wu, "Determination of the parameters representing the cross-magnetizing effect in saturated synchronous machines," *IEEE Trans. Energy Convers.*, vol. 8, no. 3, pp. 333–340, Sep. 1993.

[2] P. Vas, K. E. Hallenius, and J. E. Brown, "Cross-saturation in smooth air-gap electric machines," *IEEE Trans. Energy Convers.*, vol. 1, no. 1, pp. 103–109, Mar. 1986.

[3] A. M. EL-Serafi, A. S. Abdallah, M. K. El-Sherbiny, and E. H. Badawy, "Experimental study of the saturation and the cross-magnetizing phenomenon in saturated synchronous machines," *IEEE Trans. Energy Convers.*, vol. 3, no. 4, pp. 815–823, Dec. 1988.

[4] J. Faucher, M. Lajoie-Mazenc, and A. Chayegani, "Characterization of a closed-loop controlled current-fed machine taking into account saturation," *IEEE Trans. Ind. Appl.*, vol. 15, pp. 482–484, 1979.

[5] I. Boldea and S. A. Nasar, "A general equivalent circuit (GEC) of electrical machines including cross-coupling saturation and frequency effects," *IEEE Trans. Energy Convers.*, vol. 3, no. 3, pp. 689–695, Sep. 1988.

[6] E. Levi and V. A. Levi, "Impact of dynamic cross-saturation on accuracy of saturated synchronous machine models," *IEEE Trans. Energy Convers.*, vol. 15, no. 2, pp. 224–230, Jun. 2000.

[7] H. A. Anvari, J. Faucher, and B. Trannoy, "An investigation in the influence of a cross-coupling effect on reluctance machine performance," in *Proc. IEE Int. Conf. Electrical Machines - Design and Applications*, 1985, pp. 70–75.

[8] G. Štumberger, B. Štumberger, D. Dolinar, and A. Hamler, "Cross magnetization effect on inductances of linear synchronous reluctance motor under load conditions," *IEEE Trans. Magn.*, vol. 37, no. 5, pp. 3658–3662, Sep. 2001.

[9] R. Morales-Caporal and M. Pacas, "A predictive torque control for the synchronous reluctance machine taking into account the magnetic cross saturation," *IEEE Trans. Ind. Electron.*, vol. 54, no. 2, pp. 1161–1167, Apr. 2007.

[10] E. Levi, "Saturation modeling in d-q axis models of salient pole synchronous machines," *IEEE Trans. Energy Convers.*, vol. 14, no. 1, pp. 44–50, Mar. 1999.

[11] S. Y. Kwak, J. K. Kim, and H. K. Jun, "Characteristic analysis of multilayer-buried magnet synchronous motor using fixed permeability method," *IEEE Trans. Energy Convers.*, vol. 20, no. 3, pp. 549–555, Sep. 2005.

[12] J. H. Hu, J. B. Zou, and W. Y. Liang, "Finite element calculation of the saturation dq-axes inductance for a direct-drive PM synchronous motor considering cross-magnetization," *Proc. Power Electronics and Drive Systems*, vol. 1, pp. 677–681, Nov. 2003.

[13] S. Morimoto, Y. Takeda, T. Hirasa, and K. Taniguchi, "Expansion of operating limits for permanent magnet motor by current vector control considering inverter capacity," *IEEE Trans. Ind. Appl.*, vol. 26, no. 5, pp. 866–871, 1990.

[14] Y. S. Chen, Z. Q. Zhu, and D. Howe, "Influence of inaccuracies in machine parameters on field-weakening performance of PM brushless AC drives," in *Proc. Int. EMD Conf.*, May 1999, pp. 691–693.

[15] H. Karmaker and A. M. Knight, "Investigation and simulation of fields in large salient-pole synchronous machines with skewed stator slots," *IEEE Trans. Energy Convers.*, vol. 20, no. 3, pp. 604–610, Sep. 2005.

[16] M. A. Alhamadi and A. Demerdash, "Modeling of effects of skewing of rotor mounted permanent magnet on the performance of brushless dc motors," *IEEE Trans. Energy Convers.*, vol. 6, no. 4, pp. 721–729, Dec. 1991.

[17] X. B. Bomela and M. J. Kamper, "Effect of stator chording and rotor skewing on performance of reluctance synchronous machine," *IEEE Trans. Ind. Appl.*, vol. 38, no. 1, pp. 91–100, Jan. 2002.

[18] S. Williamson, T. J. Flack, and A. F. Volschenk, "Representation of skew in time-stepped two-dimensional finite-element models of electrical machines," *IEEE Trans. Ind. Appl.*, vol. 31, no. 5, pp. 1009–1015, Oct. 1995.

[19] H. De Gersem, K. Hameyer, and T. Weiland, "Skew interface conditions in 2-D finite-element machine models," *IEEE Trans. Magn.*, vol. 39, no. 3, pp. 1452–1455, May 2003.

[20] Y. S. Chen, Z. Q. Zhu, and D. Howe, "Calculation of d- and q-axis inductances of PM brushless ac machines accounting for skew," *IEEE Trans. Magn.*, vol. 41, no. 10, pp. 3940–3942, Oct. 2005.

[21] A. E. Fitzgerald, C. Kingsley, and S. D. Umans, *Electric Machinery*. New York: McGraw-Hill, 1989.

[22] N. Mohan, T. M. Undeland, and W. P. Robbins, *Power Electronics*. New York: Springer, 1995.

[23] Y. S. Chen, "Motor Topologies and Control Strategies for Permanent Magnet Brushless AC Drives," Ph.D. dissertation, Univ. Sheffield, Sheffield, U.K., 1999.

[24] S. Morimoto, M. Sanada, and Y. Takeda, "Effects and compensation of magnetic saturation in flux-weakening controlled permanent magnet synchronous motor drives," *IEEE Trans. Ind. Appl.*, vol. 30, no. 6, pp. 1632–1637, 1994.

[25] P. P. Silvester and R. L. Ferrari, *Finite Elements for Electrical Engineering*. Cambridge, U.K.: Cambridge Univ. Press, 1990.

[26] Z. Q. Zhu, Y. S. Chen, and D. Howe, "Online optimal flux-weakening control of permanent magnet brushless ac drives," *IEEE Trans. Ind. Appl.*, vol. 36, no. 6, pp. 1661–1668, Nov. 2000.

[27] Z. Q. Zhu, Y. S. Chen, and D. Howe, "Iron loss in PM brushless ac machines under maximum torque per ampere and flux-weakening control," *IEEE Trans. Magn.*, vol. 38, no. 5, pp. 3285–3287, Sep. 2002.

[28] L. Ma, M. Sanada, S. Morimoto, and Y. Takeda, "Prediction of iron loss in rotating machines with rotational loss included," *IEEE Trans. Magn.*, vol. 39, no. 4, pp. 2036–2041, Jul. 2003.